

Article

Ac-Susceptibility Studies of the Energy Barrier to Magnetization Reversal in Frozen Magnetic Nanofluids of Different Concentrations

Cristian E. Botez ^{1,*} and Alex D. Price ²

¹ Department of Physics and Astronomy, University of Texas at San Antonio, 1 UTSA Circle, San Antonio, TX 78249, USA

² Department of Physics, University of Texas at El Paso, 500 W. University Avenue, El Paso, TX 79968, USA; adprice.c137@gmail.com

* Correspondence: cristian.botez@utsa.edu; Tel.: +1-210-458-8227

Abstract: We used ac-susceptibility to measure the blocking temperature, T_B , and energy barrier to the magnetization reversal, E_B , of nanomagnetic fluids of different concentrations, c . We collected data on five samples synthesized by dispersing Fe_3O_4 nanoparticles of average diameter $\langle D \rangle = 8$ nm in different volumes of carrier fluid (hexane). We found that T_B increases with the increase in c , a behavior predicted by the Dormann–Bessais–Fiorani (DBF) theory. In addition, our observed T_B vs. c dependence is excellently described by a power law $T_B = A \cdot c^\gamma$, with $A = 64$ K and $\gamma = 0.056$. Our data also show that a Néel–Brown activation law $\tau(T) = \tau_0 \exp\left(\frac{E_B}{k_B T}\right)$ describes the superspin dynamics in the most diluted sample, whereas an additional energy barrier term, E_{ad} , is needed at higher concentrations, according to the DBF model: $\tau(T) = \tau_r \exp\left(\frac{E_B + E_{ad}}{k_B T}\right)$. We found $E_B/k_B = 366$ K and additional energy barriers E_{ad}/k_B that increase linearly with the common logarithm of the volume concentration, from 138 K at $c = 8.3 \times 10^{-4}\%$ to 745 K at $c = 4 \times 10^{-2}\%$. These results add to our understanding of the contributions by different factors to the superspin dynamics. In addition, the quantitative relations that we established between the T_B , E_{ad} , and c support the current efforts towards the rational design of functional nanomaterials.

Keywords: magnetic nanoparticles; superspin relaxation; blocking temperature



Citation: Botez, C.E.; Price, A.D. Ac-Susceptibility Studies of the Energy Barrier to Magnetization Reversal in Frozen Magnetic Nanofluids of Different Concentrations. *Appl. Sci.* **2023**, *13*, 9416. <https://doi.org/10.3390/app13169416>

Academic Editor: Matt Oehlschlaeger

Received: 26 July 2023

Revised: 14 August 2023

Accepted: 18 August 2023

Published: 19 August 2023



Copyright: © 2023 by the authors. Licensee MDPI, Basel, Switzerland. This article is an open access article distributed under the terms and conditions of the Creative Commons Attribution (CC BY) license (<https://creativecommons.org/licenses/by/4.0/>).

1. Introduction

The giant magnetic moment (the superspin) of a nanoparticle in an ideal, non-interacting ensemble relaxes according to the Néel–Brown model, which holds that the time (τ) it takes the superspin to flip along an easy magnetization axis depends on the temperature (T) according to an Arrhenius-type activation law [1,2]:

$$\tau(T) = \tau_0 \exp\left(\frac{E_B}{k_B T}\right) \quad (1)$$

where τ_0 is a characteristic time (typically of the order of 10^{-10} to 10^{-9} s), $k_B = 1.380649 \times 10^{-23}$ J/K is the Boltzmann constant, and E_B is the energy barrier to magnetization (superspin) reversal. At temperatures above a certain threshold, T_B (the blocking temperature), a so-called superparamagnetic transition occurs: τ becomes shorter than the observation time τ_{obs} used to perform a magnetic measurement, so the ensemble exhibits (super)paramagnetic properties although the nanoparticles' material is ferro- or ferri-magnetic. τ_{obs} is determined by the measurement type, e.g., $\tau_{obs} \sim 1$ s for dc-magnetization, while $\tau_{obs} = 1/2\pi f$ for ac-susceptibility measurements (where f is the frequency of the driving magnetic field). Therefore, the blocking temperature T_B depends on the energy barrier to superspin reversal E_B , as well as on the measurement technique.

In recent years, a lot of effort has been invested in studying the behavior of superparamagnetic nanoparticle ensembles. Both experimental and computational investigations have been carried out, and significant progress has been made in developing new and enhancing existing applications of these systems in imaging [3–5], high-density magnetic recording [6,7], and medicine [8–10]. One important observation that has emerged from these studies is that the functionality of many of the magnetic nanoparticle applications critically depends on the ability to determine and control T_B and E_B . For example, magnetic recording devices based on nanoparticle ensembles catastrophically fail (i.e., all the stored information is lost) at temperatures above T_B as the system becomes superparamagnetic [11]. For fine nanoparticles of average size smaller than 10 nm that can occur below room temperature. For medical applications, an insufficient E_B value is the main factor that prevents magnetic nanoparticles from effectively functioning as stand-alone hyperthermia cancer therapy agents [12]. Heat dissipation in superparamagnetic nanoparticle ensembles is not hysteretic but largely depends on the superspin flip across the energy barrier to magnetization reversal. For the ideal nanoparticle ensemble described above, predicting E_B and T_B is straightforward, as $E_B = KV$ and $T_B = \frac{E_B}{k_B \ln(\tau/\tau_0)}$, where K is the magneto-crystalline anisotropy constant of the material and V is the nanoparticle's volume. Real cases, however, are significantly more complicated. Even for nanoparticle ensembles with sharp size distributions and negligible interparticle interactions, measurements have revealed barriers to superspin reversal that are significantly greater than KV . This was ascribed to an additional surface component to the anisotropy constant, a hypothesis confirmed by several studies [13–15]. In commonly used nanoparticle ensembles (e.g., in nanopowders), interparticle dipolar interactions also play an important role in determining the barrier to magnetization reversal and the blocking temperature, together with other factors such as the particle size distribution, geometrical arrangements of the particles, and orientation of the easy axes [16,17].

The effect of interparticle dipolar interactions on the collective superspin relaxation has been characterized by several empirical and phenomenological models. For example, the relative peak temperature variation per frequency decade, $\phi = \frac{\Delta T}{T \cdot \Delta \log(f)}$, is typically used to assess the strength of the interparticle interactions in a magnetic nanoparticle ensemble. $\Delta T = T_2 - T_1$ is the shift of the peak temperature between two in-phase magnetic susceptibility χ' vs. $T|_f$ curves measured at different frequencies, f_1 and f_2 , of the driving magnetic field, whereas $\Delta \log(f) = \log(f_2) - \log(f_1)$. ϕ has been used to distinguish between weak interactions ($0.1 < \phi < 0.2$) leading to blocking–unblocking superparamagnetic transitions [18] and stronger interactions ($\phi < 0.05$), which can lead to the collective freezing of the superspins in a spin-glass fashion [19,20]. Within the former ϕ range, the temperature dependence of the superspin relaxation time is well described by a Vogel–Fulcher law, $\tau(T) = \tau_0 \exp\left[\frac{E_B}{k_B(T-T_0)}\right]$. This is very similar to the Néel–Brown activation law in Equation (1), with the exception of the additional parameter T_0 , which describes the strength of the interparticle interactions [21,22]. It is important to note the phenomenological nature of this description of the superparamagnetic relaxation in the presence of weak dipolar interactions. Indeed, T_0 has no physical meaning, and the exponent in the Vogel–Fulcher law diverges as T_0 increases and approaches T . The latter confirms that the law does not apply for strong interactions.

More recently, Dormann, Bessais, and Fiorani (DBF) developed a physical model for the magnetic relaxation of a nanoparticle ensemble based on a statistical calculation of the dipolar energy [23]. The DBF equation:

$$\tau(T) = \tau_r \exp\left(\frac{E_B + E_{ad}}{k_B T}\right) \quad (2)$$

introduces an additional component to the energy barrier to magnetization reversal, E_{ad} , and a variable pre-factor, τ_r . The model predicts that E_{ad} and, implicitly, T_B increase with the increase of the interparticle interactions [24,25], and, for negligible interactions

(i.e., $E_{ad} = 0$), it expectedly yields the Néel–Brown equation. Interestingly, a previous model by Mørup and Tronc (MT) based on calculations of the average dipolar field $\langle B_i \rangle$ that acts on a nanoparticle's magnetic moment μ predicts a blocking temperature T_B that actually decreases with the increasing strength of the interparticle interactions [26]. It is important to mention, however, that the predictions of the two models are not necessarily incompatible with one another, as the MT theory was developed for very weak interparticle interactions, i.e., $\mu \langle B_i \rangle \ll KV$. Experiments aimed at validating such models are difficult, as disentangling the contributions to the superspin relaxation by different factors that act in non-ideal nanoparticle ensembles—such as the bulk and surface anisotropy, interparticle dipolar interactions, geometrical arrangements, and size distributions—is a very complex task. Moreover, synthesizing solid samples (e.g., nanopowders) that allow the interparticle distance to be varied within a wide range while avoiding agglomeration and ensuring a sharp size distribution, is also particularly challenging.

Here, we used ac-susceptibility measurements to investigate the magnetic relaxation of Fe_3O_4 nanoparticles of average diameter $\langle D \rangle = 8$ nm dispersed in different volumes of a carrier fluid (hexane). By using this method, we managed to synthesize samples with low volume concentrations, c , right above the value that renders the interparticle interactions negligible ($c = 4 \times 10^{-4}\%$ v/v). Our goal was to test the predictions of the DBF model in highly diluted nanoparticle ensembles with weak interparticle dipolar interactions, which cannot be carried out using nanopowders. We used Fe_3O_4 because it represents a model system for the study of fundamental processes in magnetic nanoparticle ensembles. We collected both in-phase and out-of-phase susceptibility frequency-resolved data (χ' vs. $T|_f$ and χ'' vs. $T|_f$, respectively) upon heating on five samples of different concentrations ranging from $4 \times 10^{-4}\%$ to $4 \times 10^{-2}\%$ v/v. Our first significant finding is that the blocking temperature, T_B , obtained from the peak of the χ' vs. T curves, increases with increasing c as predicted by the DBF model. We also found that the observed T_B vs. c dependence is excellently described by a power law $T_B = A \cdot c^\gamma$, with $A = 64$ K and $\gamma = 0.056$. We then analyzed the temperature dependence of the relaxation time, $\tau(T)$, obtained from the shift with frequency of the χ'' vs. $T|_f$ data, in the framework of the DBF model. Fits of Equation (2) to the observed $\tau(T)$ datasets allowed us to determine the total energy barrier to magnetization reversal, $E_B + E_{ad}$, for the five nanoparticle ensembles of different concentrations. We found $E_B/k_B = 366$ K and a reduced additional energy barrier E_{ad}/k_B that increases linearly with the common logarithm of the volume concentration, from $c = 8.3 \times 10^{-4}\%$ to 745 K at $c = 4 \times 10^{-2}\%$. Our results are significant because they confirm the predictions of the DBF model in highly diluted ensembles of superparamagnetic nanoparticles and reveal quantitative information about the T_B vs. c dependence within this low concentration regime. They also provide a means to determine the contributions to the barrier to superspin reversal from the bulk and surface magnetocrystalline anisotropy and the interparticle interactions at different values of c . This opens new paths for the rational design of nanoparticle ensembles for magnetic recording and biomedical applications.

2. Materials and Methods

The superparamagnetic nanoparticle ensembles used in this study were prepared as follows: 10 mg of Fe_3O_4 magnetic nanoparticles of average diameter $\langle D \rangle = 8$ nm coated with oleic acid (NN Labs[®], Fayetteville, AR, USA) were initially dispersed in 5 mL of carrier fluid (hexane) to synthesize a magnetic fluid, S1, of volume concentration $c = 4 \times 10^{-2}\%$ v/v. The other four samples were prepared via progressive dilution, by adding more carrier fluid to S1. This led to nanoparticle ensembles of lower volume concentrations S2 ($c = 1.3 \times 10^{-2}\%$), S3 ($c = 1.7 \times 10^{-3}\%$), S4 ($c = 8.3 \times 10^{-4}\%$), and S5 ($c = 4 \times 10^{-4}\%$). There are two main reasons for using this method. First, it allowed us to obtain samples of low concentrations that span a broad, two-order-of-magnitude range. Second, all samples have the same average size, size distribution, and magnetic anisotropy because they come from the same powder. This is significant for the purpose of our study because the only difference between the nanoparticle ensembles used here is their interparticle distance, which governs

the strength of the interparticle dipolar interactions. The oleic acid surfactant was used to avoid particle agglomeration, and all measurements were carried out at temperatures below the freezing point of hexane, $T_F = 178$ K. This was carried out to ensure that the magnetic relaxation occurs exclusively through the Néel mechanism (the rotation of the superspin within an immobile nanoparticle), since the Brown relaxation (the rotation of the superspin together with the nanoparticle in the carrier fluid) is suppressed below T_F . Magnetic measurements were carried out using a Quantum Design[®] Physical Property Measurement System (PPMS). For each sample, ~ 0.2 mL of magnetic fluid was sealed in a polycarbonate capsule and placed in a cylindrical (0.25 cm diameter \times 1 cm height) sample holder attached to the end of a 50 cm rod. This allowed the sample to be lowered in the PPMS's cryostat and placed in the center of its pickup coil system. The temperature was then brought down to 10 K at a rate of 5 K/min. Ac-susceptibility data were collected on each of the five samples upon heating from 10 K to 150 K at a rate of 1 K/min. At each step, a 30 s delay time was used for the temperature to stabilize. For all samples, both the in-phase (χ') and out-of-phase (χ'') components of the susceptibility were recorded in a single experimental run. Measurements were performed using driving magnetic fields of amplitude $H = 50$ e and frequencies ranging from 100 Hz to 10,000 Hz.

3. Results and Discussion

Figure 1a shows the temperature dependence of the in-phase susceptibility measured on the S3 sample ($1.7 \times 10^{-3}\%$ v/v) at five different frequencies: 100 Hz, 300 Hz, 1000 Hz, 3000 Hz, and 10,000 Hz.

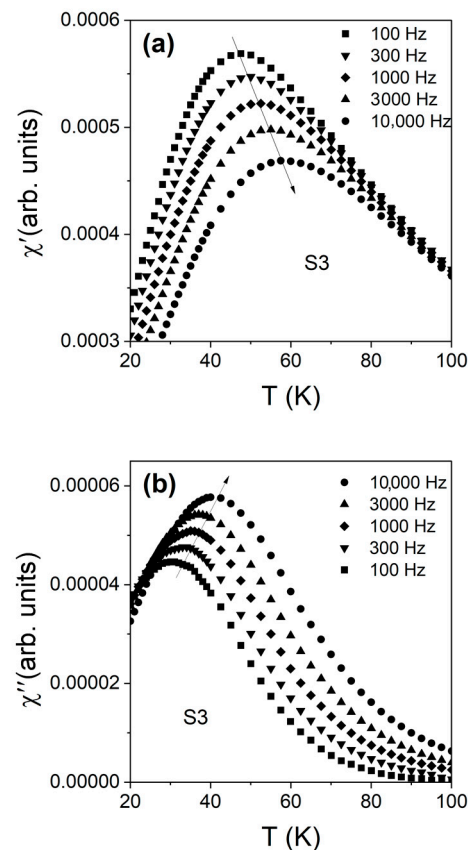


Figure 1. In-phase (a) and out-of-phase (b) components of the ac-susceptibility collected on the S3 ($c = 1.7 \times 10^{-3}\%$ v/v) sample within the 20 K–100 K temperature range at five different frequencies of the driving magnetic field: 100 Hz (squares), 300 Hz (inverted triangles), 1000 Hz (diamonds), 3000 Hz (upright triangles), and 10,000 Hz (circles).

The main feature of these χ' vs. $T|_f$ curves is that they exhibit robust peaks, whose temperature increases with the increase in the measurement frequency. This allows the calculation of the relative peak temperature variation per frequency decade, $\phi = \frac{\Delta T}{T \cdot \Delta \log(f)}$. We found $\phi = 0.15$ for the S3 sample, a value that shows the superparamagnetic nature of the transition undergone by the nanoparticle ensemble upon heating above a blocking temperature T_B that depends on the measurement frequency. Similar χ' vs. $T|_f$ data and analyses on samples S1, S2, S4, and S5 yielded ϕ values within the 0.1–0.2 range. This confirms that for all the concentrations used here, the magnetic relaxation occurs in the presence of weak interparticle interactions, and the ensembles exhibit superspin blocking–unblocking transitions. The out-of-phase susceptibility curves χ'' vs. $T|_f$ measured on sample S3 are shown in Figure 1b. The magnitudes of these curves are reversed compared to their in-phase counterparts (i.e., the χ'' vs. $T|_{10,000 \text{ Hz}}$ peak has the largest magnitude), but the peak temperature still increases with the increase in the frequency f or, equivalently, the observation time $\tau_{\text{obs}} = 1/2\pi f$. For this reason, χ'' vs. $T|_f$ curves will be used to determine the observed $\tau(T)$ dependence in each of the five nanoparticle ensembles used in this study.

To determine which model to use to analyze the observed temperature dependence of the superspin relaxation, we first studied the variation of the blocking temperature with the nanoparticle ensemble concentration, T_B vs. c . Figure 2 shows the χ' vs. $T|_{100 \text{ Hz}}$ curves measured on the five samples of different concentrations c .

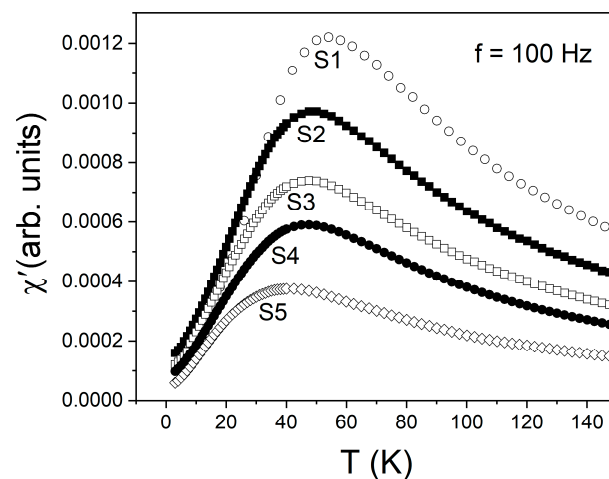


Figure 2. Temperature dependence of the in-phase susceptibility, χ' vs. T , measured at $f = 100 \text{ Hz}$ of the five samples of different volume concentrations S1, $c = 4 \times 10^{-2}\%$ (open circles), S2, $c = 1.3 \times 10^{-2}\%$ (filled squares), S3, $c = 1.7 \times 10^{-3}\%$ (open squares), S4, $c = 8.3 \times 10^{-4}\%$ (filled circles), and S5, $c = 4 \times 10^{-4}\%$ (open diamonds). The shift of the χ' peak temperature upon dilution allows the T_B vs. c dependence to be determined.

As indicated above, these curves peak at the blocking temperature corresponding to the transition from the blocked to the superparamagnetic state of the nanoparticle ensemble. Therefore, the data demonstrate that T_B increases monotonically with the increase in c , from $T_B = 39 \text{ K}$ at $c = 4 \times 10^{-4}\%$ (S5) to $T_B = 53 \text{ K}$ at $c = 4 \times 10^{-2}\%$ (S1). This is the type of behavior predicted by the DBF model, which might seem somewhat unexpected given the high level of dilution of the samples used in our work, where the concentrations are below $4 \times 10^{-2}\%$ v/v . It is worth noting, however, that denser Fe_3O_4 /hexane ferrofluids of w/v concentration 20 mg/mL (i.e., $4 \times 10^{-1}\%$ v/v) have been shown by previous studies [27] to correspond to strong interactions that lead to a collective superspin-glass-like freezing upon cooling below a critical temperature. This is markedly different from the blocking–unblocking superparamagnetic transition observed by us and cannot be analyzed in the framework of the DFB model. On the other hand, we cannot exclude a certain level of particle agglomeration upon the freezing of the carrier fluid in our studies, which is the

main reason for which we report our results in terms of the volume concentration at synthesis and not in terms of the interparticle distance calculated assuming a uniform distribution of the nanoparticles.

We then investigated the quantitative aspects of the T_B vs. c behavior. Figure 3 shows the blocking temperature measured as a function of the ferrofluid's volume concentration (solid symbols) obtained from the ac-susceptibility data in Figure 2. We made several attempts to fit these data using basic functions and found that that a power law:

$$T_B = A \cdot c^\gamma \quad (3)$$

excellently describes the observed behavior of the blocking temperature. Indeed, a least-squares fit of this newly determined equation to the T_B vs. c data converges to low residuals upon the simultaneous variation of parameters A and γ . The solid line shows the best fit that yields $A = 64$ K and $\gamma = 0.056$.

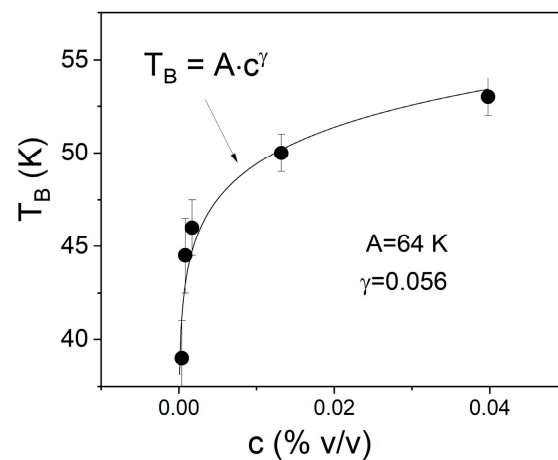


Figure 3. Blocking temperature, T_B , dependence on the concentration, c , obtained from the peak shift of the ac-susceptibility data in Figure 2 (solid symbols). The solid line shows the best fit of a power law $T_B = A \cdot c^\gamma$, with $A = 64$ K and $\gamma = 0.056$.

Next, we focus our analysis on the temperature dependence of superspin relaxation time, $\tau(T)$, for samples of different concentrations. We will then use those data to gain quantitative information on the energy barrier to magnetization reversal and finally establish how the barrier changes with the concentration. Figure 4a shows the shift with frequency of the χ'' vs. $T|_f$ curve peak temperature for the S3 sample. As the system's relaxation time, τ , is the same as the observation time, τ_{obs} , (i.e., $\tau = \tau_{\text{obs}} = 1/2\pi f$) at the peak temperature, these curves allow us to determine the $\tau(T)$ dependence for the S3 sample. This is shown by the solid symbols in Figure 4b, where the natural logarithm of τ is plotted as a function of inverse temperature $1/T$. We then analyzed these data in the framework of the DBF theory. We used Equation (2), where the relaxation time is calculated based on three quantities: the pre-factor τ_r , the energy barrier for the individual nanoparticle relaxation according to the Néel and Brown model E_B , and the additional energy barrier, E_{ad} , which corresponds to the collective superspin relaxation due to interparticle interactions. Two parameters, τ_r and E_{ad} , were allowed to vary simultaneously in the fit of the DBF equation to the data, while E_B/k_B was kept at 366 K for reasons explained below. The best fit, shown by the solid line, converges to low residuals and yields $\tau_r = 1.1 \times 10^{-12}$ s and $E_{\text{ad}}/k_B = 289$ K.

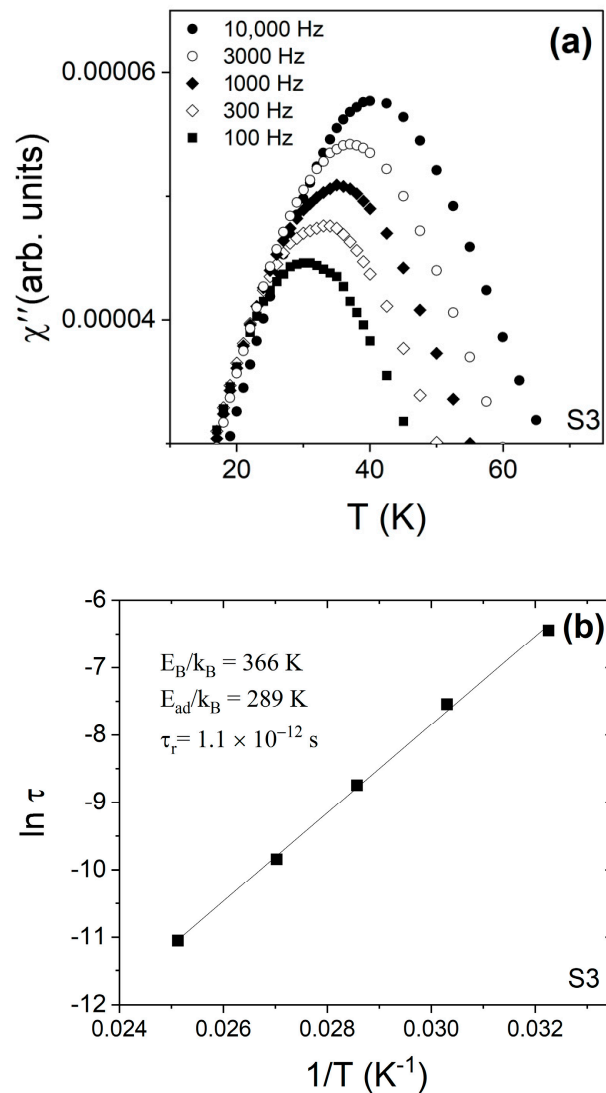


Figure 4. (a) Temperature dependence of the out-of-phase susceptibility, χ'' vs. T , measured on the S3 ($c = 1.7 \times 10^{-3}\%$ v/v) sample at different frequencies: 100 Hz (filled squares), 300 Hz (open diamonds), 1000 Hz (filled diamonds), 3000 Hz (empty circles), and 10,000 Hz (filled circles). (b) Temperature dependence of the relaxation time, τ , (solid symbols) obtained from ac-susceptibility data and best fit of the DBS model equation $\tau(T) = \tau_r \exp\left(\frac{E_B + E_{ad}}{k_B T}\right)$ (solid line).

We determined the individual energy barrier to magnetization reversal, E_B , as follows. For the lowest concentration, sample S5 ($c = 4 \times 10^{-4}\%$), we managed to successfully fit the observed $\tau(T)$ behavior using the Néel–Brown equation $\tau(T) = \tau_0 \exp\left(\frac{E_B}{k_B T}\right)$ with parameters $\tau_0 = 5.6 \times 10^{-10}$ s and $E_B/k_B = 366$ K. This is significant because it indicates that the Fe_3O_4 nanoparticle ensemble in S5 is diluted enough, so each particle relaxes individually across an energy barrier, E_B , that only depends on the bulk and surface magnetic anisotropy. The key value that supports this conclusion is the vertical axis intercept of the $\ln \tau$ vs. $1/T$ dependence, $\ln \tau_0$, which in this case yields a τ_0 between 10^{-9} and 10^{-11} s. Values of the inverse attempt frequency ($\tau_0 = 1/2\pi f_0$) within this range are a known signature of non-interacting nanoparticle ensembles where each superspin relaxes independently [20,27]. In addition, we note that E_B/k_B has the same value in all five samples because they were prepared by progressively diluting the same nanopowder.

Figure 5 shows the temperature dependence of the relaxation time measured on samples S1 (upright triangles), S2 (diamonds), S3 (inverted triangles), S4 (circles), and S5 (squares), using χ'' vs. $T|_f$ data, such as the ones in Figure 4a. The main feature here is

that the slope of the $\ln\tau$ vs. $1/T$ plots increases with the increase in c , indicating that the superspin needs to overcome a higher energy barrier in denser samples. The solid lines are best fits of Equation (2), which allow the energy barrier to superspin reversal $E_B + E_{ad}$ to be determined. As discussed above, we found $E_{ad} = 0$ K and $E_B/k_B = 366$ K for the S5 sample. For the other four samples, the best fits yield additional energy barriers that increase with the increase in concentration, from $E_{ad}/k_B = 138$ K for S4 ($c = 8.3 \times 10^{-4}\%$) to $E_{ad}/k_B = 745$ K for S1 ($c = 4 \times 10^{-2}\%$). These results are summarized in the inset table and shown by the solid symbols in Figure 6. The solid line here is a guide to the eye showing that the additional barrier to superspin reversal, E_{ad}/k_B , increases linearly with the common logarithm of the concentration $\log_{10}c$. We note that upon the increase in the volume concentration, the additional energy barrier reaches values comparable to its E_B/k_B counterpart at $c \sim 5 \times 10^{-3}\%$. For sample S1, we found $E_{ad}/k_B > 2E_B/k_B$, which clearly demonstrates the strong effect of the interparticle interactions even at low nanoparticle volume concentrations, below $10^{-1}\%$. At the microscopic level, the observed dependence of the barrier to magnetization reversal on concentration indicates that, up to $c = 4 \times 10^{-4}\%$, the nanoparticles' magnetic moments (the superspins) only need to overcome E_B (i.e., the barrier resulting from the bulk and surface magneto-crystalline anisotropy) in order to flip along an easy magnetization axis via thermal activation. This is the same as the case of an isolated magnetic nanoparticle, as described by the Néel–Brown model. Further increasing the concentration leads to non-negligible magnetic dipolar interactions among the nanoparticles in the ensemble. This collective relaxation requires more energy for the superspin flips. In the DBS model, this is equivalent to an additional energy barrier to superspin reversal that increases with the concentration and becomes dominant above $c = 4 \times 10^{-4}\%$.

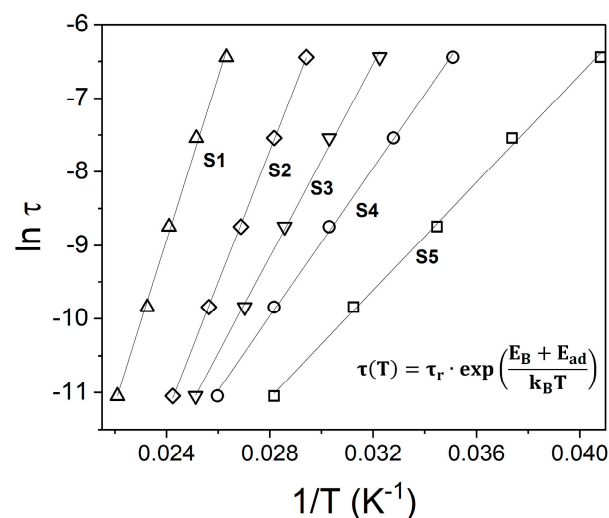


Figure 5. Temperature dependence of the relaxation time, τ , obtained from ac-susceptibility data collected on samples of different volume concentrations S1, $c = 4 \times 10^{-2}\%$ (upright triangles), S2, $c = 1.3 \times 10^{-2}\%$ (diamonds), S3, $c = 1.7 \times 10^{-3}\%$ (inverted triangles), S4, $c = 8.3 \times 10^{-4}\%$ (circles), and S5, $c = 4 \times 10^{-4}\%$ (squares). The solid lines are best fits to the DBS model with $E_B/k_B = 366$ K.

Our findings are significant for several reasons. First, they demonstrate that despite the high dilution level ($4 \times 10^{-2}\% \geq c \geq 8.3 \times 10^{-4}\%$), samples S1–S4 still exhibit a collective relaxation of the superspins, which is typically indicative of interparticle interactions. This is unequivocally confirmed by the existence of the additional energy barrier to magnetization reversal E_{ad} that increases with the increase in c . The ability to identify the concentration range where this behavior occurs is a new result that is particularly important for applications of magnetic nanoparticles in high-density magnetic recording, where each superspin acts as one recording bit that needs to flip individually. Second, our observation that the nanoparticles in sample S5 relax individually allowed us to determine E_B and, more

importantly, separate the E_B and E_{ad} components in the denser samples. This is important because it adds to our understanding of the contributions of different factors that influence the superspin relaxation, such as bulk and surface magnetic anisotropy, nanoparticle size and size distribution, and interparticle interactions. Finally, the quantitative relations that we established between the blocking temperature, additional energy barrier to magnetization reversal, and nanoparticle concentration are significant for the current efforts to design functional nanomaterials using a rational approach instead of the common trial and error method.

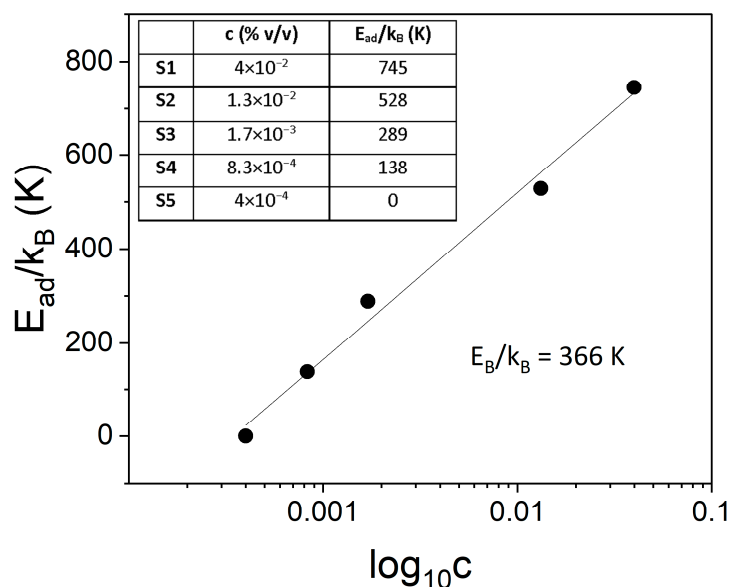


Figure 6. Concentration dependence of the reduced additional energy barrier to magnetization reversal E_{ad}/k_B (solid symbols) obtained from the DBF analysis in Figure 5. E_{ad}/k_B increases linearly with the common logarithm of the concentration (solid line).

Further work will be aimed at investigating the interplay between the Néel and the Brown superspin relaxation mechanisms at temperatures above the melting point of the carrier fluid. Such studies are important because they enhance the knowledge needed to advance magnetic nanoparticle hyperthermia from its current adjunct-to-other-treatments status to a powerful stand-alone cancer therapy. Our experimental strategy will be to increase the average size of the nanoparticle ensembles so that the superparamagnetic unblocking occurs at temperatures above the freezing point of the carrier fluid. In addition, we will use ensembles of different concentrations to vary the interparticle dipolar interactions, and carrier fluids of different viscosities to vary the energy barrier to physical rotation that governs the Brown relaxation. These experiments are currently underway.

4. Conclusions

We used ac-susceptibility to measure the blocking temperature, T_B , and energy barrier to magnetization reversal, E_B , in highly diluted magnetic fluids synthesized by dispersing 8 nm-diameter Fe_3O_4 nanoparticles in hexane. Data collected on five samples of volume concentrations (v/v) of $4 \times 10^{-2}\%$, $1.3 \times 10^{-2}\%$, $1.7 \times 10^{-3}\%$, $8.3 \times 10^{-4}\%$, and $4 \times 10^{-4}\%$, show that, in each case, the system undergoes superparamagnetic transitions. The corresponding blocking temperatures increase with the increase in concentration, from $T_B = 39$ K at $c = 4 \times 10^{-4}\%$ to $T_B = 53$ K at $c = 4 \times 10^{-2}\%$, according to a power law $T_B = A \cdot c^\gamma$, with $A = 64$ K and $\gamma = 0.056$. As a monotonic increase in T_B with c was predicted by the Dormann–Bessais–Fiorani (DBS) model, we used the DBS equation, $\tau(T) = \tau_r \exp\left(\frac{E_B + E_{ad}}{k_B T}\right)$ to analyze the observed superspin relaxation behaviors, $\tau(T)$, of the nanomagnetic fluids. Expectedly, we found $E_{ad} = 0$ for the lowest concentration sample ($c = 4 \times 10^{-4}\%$), which allowed us to determine $E_B/k_B = 366$ K. We used this value

to determine the additional energy barriers E_{ad}/k_B in the denser samples. We found that E_{ad}/k_B increases linearly with the common logarithm of the volume concentration, from 138 K at $c = 8.3 \times 10^{-4}\%$ to 745 K at $c = 4 \times 10^{-2}\%$.

Author Contributions: C.E.B.: conceptualization, methodology, investigation, project administration, formal analysis, and writing—original draft. A.D.P.: methodology, formal analysis, investigation, and writing—review, and editing. All authors have read and agreed to the published version of the manuscript.

Funding: This research was funded in part by the U.S. Department of Defense Army Research Office under Award No. 64705CHREP.

Institutional Review Board Statement: Not applicable.

Informed Consent Statement: Not applicable.

Data Availability Statement: The data presented in this study are available from the corresponding author upon reasonable.

Conflicts of Interest: The authors declare no conflict of interest.

References

1. Neel, L. Théorie du traînage magnétique des ferromagnétiques en grains fins avec application aux terres cuites. *Ann. Géophysique* **1949**, *5*, 99–136.
2. Brown, W.F. Thermal fluctuations of a single-domain particle. *Phys. Rev.* **1963**, *130*, 1677–1686. [[CrossRef](#)]
3. Beg, M.S.; Mohapatra, J.; Pradhan, L.; Patkar, D.; Bahadur, D. Porous Fe₃O₄-SiO₂ Core-Shell Nanorods as High-Performance MRI Contrast Agent and Drug Delivery Vehicle. *J. Magn. Magn. Mater.* **2017**, *428*, 340–347. [[CrossRef](#)]
4. Wang, X.; Pan, F.; Xiang, Z.; Jia, W.; Lu, W. Magnetic Fe₃O₄@PVP Nanotubes with High Heating Efficiency for MRI-Guided Magnetic Hyperthermia Applications. *Mater. Lett.* **2020**, *262*, 127187. [[CrossRef](#)]
5. Wang, L.; Neoh, K.G.; Kang, E.T.; Shuter, B.; Wang, S.-C. Superparamagnetic Hyperbranched Polyglycerol-Grafted Fe₃O₄ Nanoparticles as a Novel Magnetic Resonance Imaging Contrast Agent: An In Vitro Assessment. *Adv. Funct. Mater.* **2009**, *19*, 2615–2622. [[CrossRef](#)]
6. Kikitsu, A. Prospects for Bit Patterned Media for High-Density Magnetic Recording. *J. Magn. Magn. Mater.* **2009**, *321*, 526–530. [[CrossRef](#)]
7. Nakamura, T.; Miyamoto, T.; Yamada, Y. Complex permeability spectra of polycrystalline Li–Zn ferrite and application to EM-wave absorber. *J. Magn. Magn. Mater.* **2003**, *256*, 340–347. [[CrossRef](#)]
8. Jordan, A.; Scholz, R.; Wust, P.; Schirra, H.; Thomas, S.; Schmidt, H.; Felix, R. Endocytosis of Dextran and Silan-Coated Magnetite Nanoparticles and the Effect of Intracellular Hyperthermia on Human Mammary Carcinoma Cells in Vitro. *J. Magn. Magn. Mater.* **1999**, *194*, 185–196. [[CrossRef](#)]
9. Hergt, R.; Dutz, S.; Müller, R.; Zeisberger, M. Magnetic Particle Hyperthermia: Nanoparticle Magnetism and Materials Development for Cancer Therapy. *J. Phys. Condens. Matter* **2006**, *18*, S2919–S2934. [[CrossRef](#)]
10. Niculaes, D.; Lak, A.; Anyfantis, G.C.; Marras, S.; Laslett, O.; Avugadda, S.K.; Cassani, M.; Serantes, D.; Hovorka, O.; Chantrell, R.; et al. Asymmetric Assembling of Iron Oxide Nanocubes for Improving Magnetic Hyperthermia Performance. *ACS Nano* **2017**, *11*, 12121–12133. [[CrossRef](#)]
11. Bedanta, S.; Barman, A.; Kleemann, W.; Petracic, O.; Seki, T. Magnetic nanoparticles: A subject for both fundamental research and applications. *J. Nanomater.* **2013**, *2013*, 952540. [[CrossRef](#)]
12. Galindo, J.T.E.; Adair, A.H.; Botez, C.E.; Flores, V.C.; Baques, D.B.; Cobas, L.F.; Matutes-Aquino, J.A. Zn-doping effect on the energy barrier to magnetization reversal in superparamagnetic nickel ferrite nanoparticles. *Appl. Phys. A* **2007**, *87*, 743–747. [[CrossRef](#)]
13. Bødker, F.; Mørup, S.; Linderroth, S. Surface effects in metallic iron nanoparticles. *Phys. Rev. Lett.* **1994**, *72*, 282–285. [[CrossRef](#)]
14. Respaud, M.; Broto, J.M.; Rakoto, H. Surface effects on the magnetic properties of ultrafine cobalt particles. *Phys. Rev. B* **1998**, *57*, 2925. [[CrossRef](#)]
15. Gilmore, K.; Idzerda, Y.U.; Klem, M.T.; Allen, M.; Douglas, T.; Young, M. Surface contribution to the anisotropy energy of spherical magnetite particles. *J. Appl. Phys.* **2005**, *97*, 10B301. [[CrossRef](#)]
16. Laureti, S.; Varvaro, G.; Testa, A.M.; Fiorani, D.; Agostinelli, E.; Piccaluga, G.; Musinu, A.; Ardu, A.; Peddis, D. Magnetic Interactions in Silica Coated Nanoporous Assemblies of CoFe₂O₄ Nanoparticles with Cubic Magnetic Anisotropy. *Nanotechnology* **2010**, *21*, 315701. [[CrossRef](#)]
17. Salvador, M.; Nicolao, L.; Figueiredo, W. Magnetic relaxation of a system of interacting magnetic nanoparticles at finite temperature. *Phys. B Condens. Matter* **2023**, *649*, 414497. [[CrossRef](#)]
18. Tackett, R.J.; Parsons, J.G.; Machado, B.I.; Gaytan, S.M.; Murr, L.E.; Botez, C.E. Evidence of low-temperature superparamagnetism in Mn₃O₄ nanoparticle ensembles. *Nanotechnology* **2010**, *21*, 365703. [[CrossRef](#)] [[PubMed](#)]

19. Botez, C.E.; Adair, A.H.; Tackett, R.J. Evidence of Superspin-Glass Behavior in $\text{Zn}_{0.5}\text{Ni}_{0.5}\text{Fe}_2\text{O}_4$ Nanoparticles. *J. Phys. Condens. Matter* **2015**, *27*, 076005. [[CrossRef](#)]
20. Tackett, R.J.; Bhuiya, A.W.; Botez, C.E. Dynamic Susceptibility Evidence of Surface Spin Freezing in Ultrafine NiFe_2O_4 Nanoparticles. *Nanotechnology* **2009**, *20*, 445705. [[CrossRef](#)]
21. Shtrikman, S.; Wohlfarth, E.P. The Theory of Vogel-Fulcher Law of Spin Glasses. *Phys. Lett. A* **1981**, *85*, 467. [[CrossRef](#)]
22. Thanh, T.D.; Manh, D.H.; Phan, T.L.; Phong, P.T.; Hung, L.T.; Phuc, N.X.; Yu, S.C. Coexistence of considerable inter-particle interactions and spin-glass behavior in $\text{La}_{0.7}\text{Ca}_{0.3}\text{MnO}_3$ nanoparticles. *J. Appl. Phys.* **2014**, *115*, 17B504. [[CrossRef](#)]
23. Dormann, J.L.; Bessais, L.; Fiorani, D. A dynamic study of small interacting particles: Superparamagnetic model and spin-glass laws. *J. Phys. C* **1988**, *21*, 2015. [[CrossRef](#)]
24. Dormann, J.L.; Fiorani, D.; Tronc, E. Magnetic Relaxation in Fine-Particle Systems. *Adv. Chem. Phys.* **1997**, *98*, 283–494.
25. De Torro, J.A.; Gonzalez, J.A.; Normile, P.S.; Muniz, P.; Andres, J.P.; Anton, R.L.; Canales-Vazquez, J.; Riveiro, J.M. Energy barrier enhancement by weak magnetic interactions in Co/Nb granular films assembled by inert gas condensation. *Phys. Rev. B* **2012**, *85*, 054429. [[CrossRef](#)]
26. Mørup, S.; Tronc, E. Superparamagnetic Relaxation of Weakly Interacting Particles. *Phys. Rev. Lett.* **1994**, *72*, 3278. [[CrossRef](#)]
27. Morales, M.B.; Phan, M.H.; Pal, S.; Frey, N.A.; Srikanth, H. Particle Blocking and Carrier Fluid Freezing Effects on the Magnetic Properties of Fe_3O_4 -based Ferrofluids. *J. Appl. Phys.* **2009**, *105*, 07B511. [[CrossRef](#)]

Disclaimer/Publisher’s Note: The statements, opinions and data contained in all publications are solely those of the individual author(s) and contributor(s) and not of MDPI and/or the editor(s). MDPI and/or the editor(s) disclaim responsibility for any injury to people or property resulting from any ideas, methods, instructions or products referred to in the content.